ISSN 1063-7834, Physics of the Solid State, 2022, Vol. 64, No. 11, pp. 576–586. © Pleiades Publishing, Ltd., 2022.
ISSN 1063-7834, Physics of the Solid State, 2022. © Pleiades Publishing, Ltd., 2022.
Russian Text © The Author(s), 2023, published in Fizika Tverdogo Tela, 2023, Vol. 65, No. 2, pp. 328–338.

Ab Initio Simulation of Dielectric and Optical Properties of Ices I_h and I_{II} and Lattice Frameworks of Hydrates sI and sH

M. B. Yunusov[a, *] and R. M. Khusnutdinoff[a, b]

[a] *Kazan (Volga Region) Federal University, Kazan, Russia*

[b] *Udmurt Federal Research Center, Ural Branch, Russian Academy of Sciences, Izhevsk, Russia*

**e-mail: mukhammadbek@mail.ru*

Received November 2, 2022; revised November 16, 2022; accepted November 16, 2022

Abstract—In this study, the results of calculating the dielectric and optical characteristics of solid polymorphic phases of water—namely, ices I_h and I_{II}, and lattice frameworks of hydrates sI and sH—are described. Static dielectric tensors ε_{ik} and complex frequency-dependent tensors $\varepsilon_{ik}(\omega)$ are calculated for these materials. It is shown that the lattices of I_h, I_{II}, and sH correspond to uniaxial crystals according to their optical properties, their $\varepsilon_{xx}(\omega)$ and $\varepsilon_{yy}(\omega)$ tensor components are identical, and the lattice of hydrate sI corresponds to an isotropic crystal. Based on calculated frequency-dependent dielectric functions $\varepsilon'_{ik}(\omega)$ and $\varepsilon''_{ik}(\omega)$, the following important optical characteristics are obtained: reflection $R(\omega)$, absorption $a(\omega)$, loss function $L(\omega)$, and refractive indices $n(\omega)$ and $k(\omega)$. Comparison of the dielectric and optical spectra of the sI and sH lattice frameworks with the known spectra for methane hydrate sI reveal a broadening of the spectra toward high-energy fields. For unfilled hydrate sI, a reflection peak at an energy of 17.3 eV is found, the appearance of which is associated with a change in the electronic structure of the crystal in the absence of a methane molecule. Qualitative agreement of reflection spectra $R(\omega)$ and the $\varepsilon'_{ik}(\omega)$ and $\varepsilon''_{ik}(\omega)$ functions calculated by quantum mechanical simulation with experimental data on the spectroscopy of the hexagonal and amorphous ice phases is obtained.

Keywords: ice, hydrate, dielectric tensor, optical functions

DOI: 10.1134/S1063783422110142

1. INTRODUCTION

Polymorphic modifications of the solid phase of water are among the most common materials on Earth and have unique physical properties [1, 2]. Ice alone exhibits at least seventeen crystalline phases that differ in structure and proton distribution [1]. Water skeletons of gas hydrates can also be referred to polymorphic modifications of ice [2]. Despite the fact that hydrates, unlike ices, are complex compounds whose crystal lattice can contain low molecular weight gases, their mechanical, thermal, optical, and electronic characteristics are close to those of ices. Ice I_h is the most widespread solid water modification in nature (Figs. 1a and 1b). Water molecules of this modification of ice are organized in an ordered hexagonal lattice, oxygen atoms form an ordered structure that resembles a honeycomb, and the arrangement of hydrogen atoms is determined by the Bernal–Fowler ice rule [3]. For ice I_h, the Bernal–Fowler rule admits a set of energy-identical proton distribution configurations in the lattice; therefore, this structure is a proton-disordered structure. Ice I_{II} (Figs. 1c and 1d) can be obtained by compressing hexagonal ice under pressures of $p \in [0.2; 0.5]$ GPa [4]. This modification of ice is a unique one, since it has an ordered arrangement of protons, which is not typical for polymorphic modifications that exist at low pressures (<20 GPa). The crystal lattice of ice I_{II} corresponds to a trigonal structure. Parallel hexagonal channels in ice I_{II}, like molecular cavities in gas hydrates, can include guest molecules—for example, molecules of hydrogen or helium—up to 3.5 Å in size [5]. Thermobaric conditions and the gas composition of the Earth's interior are optimal for the formation of gas hydrates with hexagonal lattice sH and with cubic lattices sI and sII. The crystal lattice of these nonstoichiometric compounds is comprised of spherical or ellipsoidal molecular cavities formed by hydrogen bonds between water molecules [6]. In natural gas hydrates, molecular cavities are filled with light gases CH_4, H_2S, H_2, N_2, Ar, Kr, Xe, CO_2, C_2H_6, and C_3H_6, whose molecules stabilize the water lattice of hydrates through the van der Waals interactions [7, 8]; the unfilled clathrate has a metastable framework. The sH hydrate modification has a hexagonal structure (Figs. 1e and 1f) and includes the following two types of water cavities: small ones ($r \approx$ 4–5 Å) and large ones ($r \approx$ 7–9 Å). Hydrate sI is the

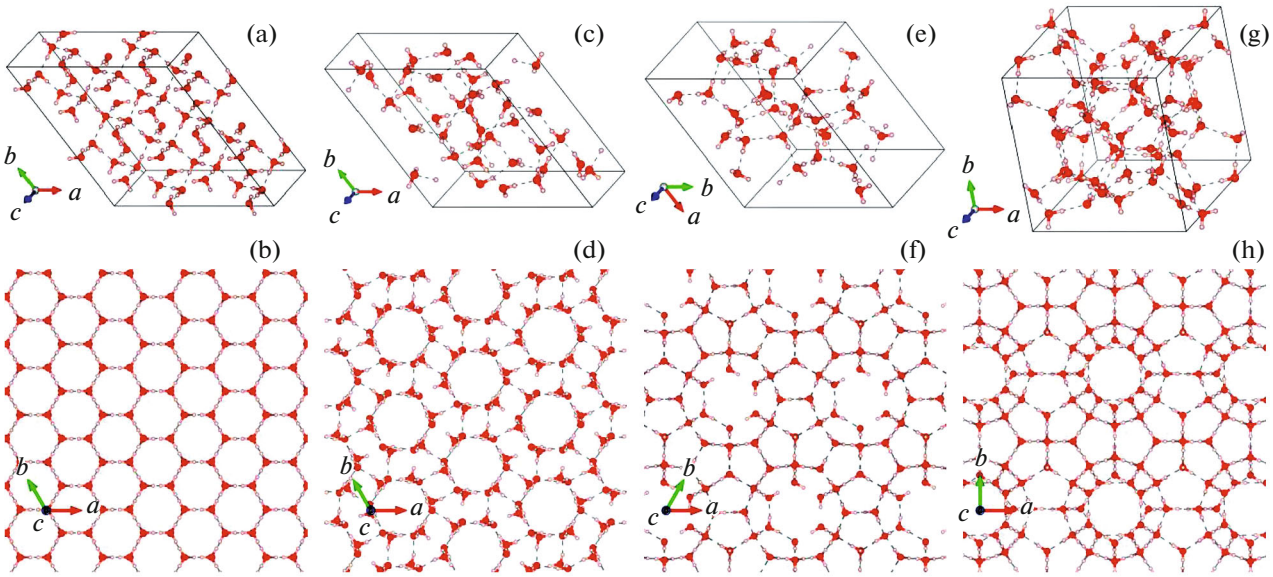

Fig. 1. Simulation cells and crystal lattices of ices (a, b) I_h and (c, d) I_{II}, frameworks of hydrates (e, f) sH and (g, h) sI.

most abundant on Earth and has a cubic structure (Figs. 1g and 1h). This modification is of particular interest for research, since gas hydrates containing hydrocarbons (methane and ethane) have the sI lattice with molecular cavities with a radius of $r \approx 5$–6 Å and a proton disordered structure, which means that there is no fixed arrangement of protons in the crystal.

The increased interest in the study of various characteristics of clathrate systems is associated with the wide prospects for their application. For example, 1 m^3 of hydrate can contain 160 m^3 of methane [9], which gives grounds to consider hydrates as natural reservoirs for storing and transporting gases [10]. Economic interest in natural gas hydrates is also due to the presence of huge reserves of methane (up to 10^{18} m^3) contained in gas hydrate deposits in the bowels of Earth [2]. A lot of studies—both experimental and theoretical—have been devoted to thermophysical and mechanical properties, and to nucleation and dissociation processes of ices and hydrates [1–5, 8–12]. At the same time, the electronic [13, 14], dielectric, and optical properties [15–21] of aqueous crystal lattices of ices and hydrates—which are not only of fundamental but also of great practical importance—are less studied. Data on the dielectric and optical properties of clathrate systems make it possible to improve electromagnetic methods for detecting and analyzing gas hydrate deposits. For example, the method of controlled source electromagnetic survey (MCSEM), which provides information about the electrical resistivity of formations up to 4 km in depth, can determine the presence of gas hydrate deposits in the rock [15], and the time domain reflectometry (TDR) method allows one to measure the concentration of gas hydrate based on bulk dielectric properties [16]. At the same time, it is also important to know the optical spectra of ice in order to distinguish gas hydrate deposits from ice reservoirs that do not contain natural gas. In [17], dielectric coefficients and optical spectra of hydrate sI filled with methane were obtained by ab initio simulation. It was shown that the absence of methane in some lattice cells of water has a little effect on the optical and electrical characteristics. In [18–20], absorption values, refractive indices, and also temperature dependences of the dielectric properties of ices and hydrates with tetrahydrofuran, methane, propane, and sulfur hexafluoride were measured by the experimental method of terahertz spectroscopy (TDS) with characteristic frequencies of electromagnetic radiation in the range of $\nu \in [0.1; 30]$ THz. In [21], the reflection and absorption spectra and dielectric functions of hexagonal (I_h) and amorphous ices in the energy range of $E \in [5; 28]$ eV were measured at 80 K by optical and photoelectron spectroscopy.

In this work, the dielectric and optical properties of ice modifications I_h and I_{II}, and clathrate frameworks sI and sH are studied using the density functional theory [22, 23], which is a high-precision ab initio method, within the pseudopotential approach in the VASP software package [24, 25]. The dielectric tensor components, the real and imaginary parts of complex dielectric functions, the optical absorption and reflection spectra, the loss functions, and the refractive indices are calculated. Since these are the first results of a quantum mechanical study of the dielectric functions of the solid phases of water, the data obtained in this study are of great theoretical and applied importance and can contribute to the development of technologies for localization and analysis of gas hydrate deposits.

Table 1. Parameters of simulation cells and crystal lattices

	N, H_2O	α, deg	β, deg	Γ, deg	a, Å	b, Å	c, Å	Space group
I_h	48	90	90	120	15.2	15.2	7.14	$P6_3/mmc$ [1, 12]
I_{II}	36	90	90	120	13.0	13.0	6.25	R-3 [1, 12]
sH	34	90	90	60	12.2	12.2	10.1	$P6/mmm$ [9, 12]
sI	46	90	90	90	12.0	12.0	12.0	Pm-3n [9, 11]

2. CRYSTAL STRUCTURE OF HYDRATES AND ICES

Dielectric and optical characteristics were calculated for the following four crystalline phases of water: ices I_h and I_{II}, and lattice frameworks of hydrates sH and sI. The simulation cells and crystal lattices for each of the considered systems are shown in Fig. 1. Table 1 gives some characteristics of the simulated systems.

3. SIMULATION DETAILS

The dielectric and optical characteristics were studied using the density functional method [22, 23], which makes it possible to calculate the microscopic and macroscopic parameters of the system based on the electron charge density distribution. When performing calculations using this method, The VASP software package, which is a specialized computer program for ab initio simulation, was used [24, 25]. To describe electron–ion interactions, the VASP algorithms use the pseudopotential method, which makes it possible to increase the efficiency of calculations by smoothing rapidly oscillating wave functions of electrons near atomic nuclei. In these calculations, the method of projected plane waves (PAW potential) [26] was used. The number of plane waves in the basis set was determined by a cutoff energy of 400 eV and ranged from 130 thousand to 230 thousand, depending on the simulated crystal. The exchange correlation interaction of electrons was taken into account using the generalized gradient approximation (GGA-PBE) [26, 27]. The system energy optimization procedure was carried out using the RMM-DIIS algorithm [28] and an energy convergence of 10^{-4} eV was achieved. The method of partitioning the inverse k-space with a grid of $2 \times 2 \times 2$ was chosen to optimize unit cells. To avoid undesirable effects associated with the finite dimensions of the simulated crystal cells, periodic boundary conditions were used.

4. DIELECTRIC TENSOR

Dielectric tensor $\varepsilon_{ik}(\omega)$ and its complex frequency-dependent components describe the propagation of electromagnetic waves in an anisotropic dielectric medium, and establish the following relationship between induction and electromagnetic field strength:

$$D_i = \varepsilon_{ik}(\omega)E_k. \quad (1)$$

Static dielectric tensor ε_{ik}, which is also called the permittivity, is a tensor for limiting case $\omega \to 0$ and describes the field in the volume of a dielectric placed in an external static electric field. According to [29], the $\varepsilon_{ik}(\omega)$ tensor is characterized by symmetry in the i and k indices.

At the first stage of the study, static macroscopic permittivity tensor ε_{ik} was calculated for each crystalline phase of water (see Table 2). Crystals I_h and sH belong to hexagonal systems, and crystal I_{II} has a trigonal structure; therefore, these crystals are uniaxial with respect to the dielectric tensor and, consequently, to optical properties. Moreover, the principal optical axes (ε_{zz}) of the dielectric tensors of the I_h, I_{II}, and sH systems coincide with vectors c in Fig. 1. The other optical axes (ε_{xx} and ε_{yy}) lie in the plane perpendicular to ε_{zz} and, according to [29], the ε_{xx} and ε_{yy} values of must match. In turn, the sI crystal has a cubic lattice according to the dielectric tensor and optical properties. The principal components of the dielectric tensor for the sI system must coincide ($\varepsilon_{zz} = \varepsilon_{xx} = \varepsilon_{yy}$), i.e., the system must have optical isotropy. The calculated values of static dielectric components ε_{zz}, ε_{xx}, and ε_{yy} (Table 2) confirm the earlier theoretical conclusions. Insignificant errors in the values of the components of dielectric tensors ε_{ik} for hydrates sI and sH are due to the fact that a less accurate electron minimization algorithm in the VASP software package was used for quantum mechanical calculations because of the complexity of these systems [24, 25]. In addition, the systems under study have a center of spatial symmetry and do not exhibit natural optical activity or gyrotropy [29].

At the next stage of the study, the frequency-dependent components of dielectric tensor $\varepsilon_{ik}(\omega)$ were calculated, which characterize the propagation of electromagnetic waves along various directions in a dielectric medium (see Fig. 2). In the general case, the $\varepsilon_{ik}(\omega)$ components are complex values:

$$\varepsilon_{ik}(\omega) = \varepsilon'_{ik}(\omega) + i\varepsilon''_{ik}(\omega). \quad (2)$$

However, the imaginary parts are equal to zero in the limiting case with $\omega \to 0$, as shown in Fig. 2. For each

Table 2. Calculated components ε_{ik} of the static dielectric tensors of ices I_h and I_{II}, and lattice frameworks of hydrates sI and sH (the z axes are aligned with vectors **c** of the unit cells shown in Fig. 1)

	ε_{xx}	ε_{yy}	ε_{zz}
Ice I_h	1.879	1.879	1.887
Ice I_{II}	2.013	2.013	2.041
Hydrate sH	1.609 ± 0.001	1.609 ± 0.001	1.620
Hydrate sI	1.626 ± 0.002	1.626 ± 0.002	1.626 ± 0.002

considered system, only the diagonal components of the tensor have nonzero values. Moreover, the values of the $\varepsilon_{xx}(\omega)$ and $\varepsilon_{yy}(\omega)$ components are identical for crystals I_h, I_{II}, and sH. For an sI crystal, $\varepsilon_{xx}(\omega) = \varepsilon_{yy}(\omega) = \varepsilon_{zz}(\omega)$.

The dielectric functions of the studied modifications of ices and hydrates behave similarly in their dependences on the frequency of the applied electromagnetic field. The $\varepsilon'_{ik}(\omega)$ and $\varepsilon''_{ik}(\omega)$ dependences for ices and hydrates show qualitative similarity, and the positions of their extrema coincide; however, the peaks of the dielectric functions have different intensities. The real $\varepsilon'_{ik}(\omega)$ functions, which describe the propagation and behavior of radiation inside the mate-

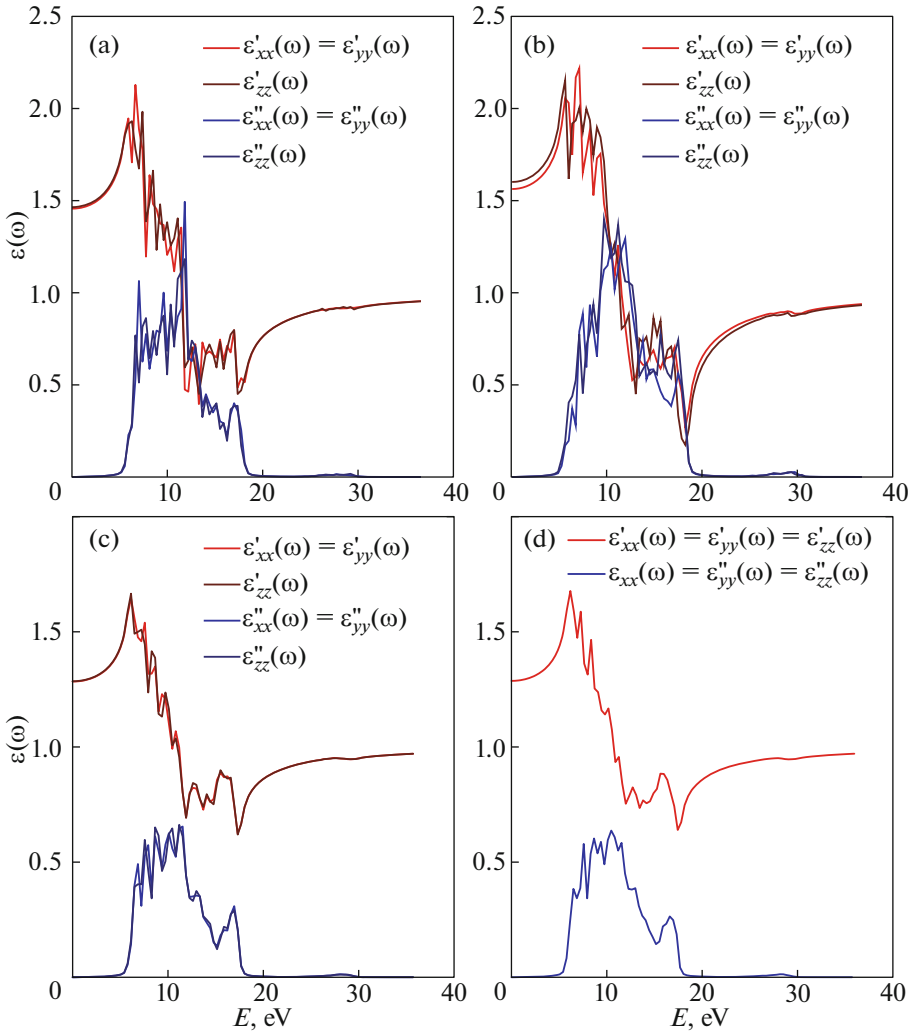

Fig. 2. Dependences of the energy of electromagnetic radiation on the real and imaginary parts of diagonal components $\varepsilon_{ik}(\omega)$ of the dielectric tensor for ices (a) I_h and (b) I_{II}, and hydrates (c) sH and (d) sI.

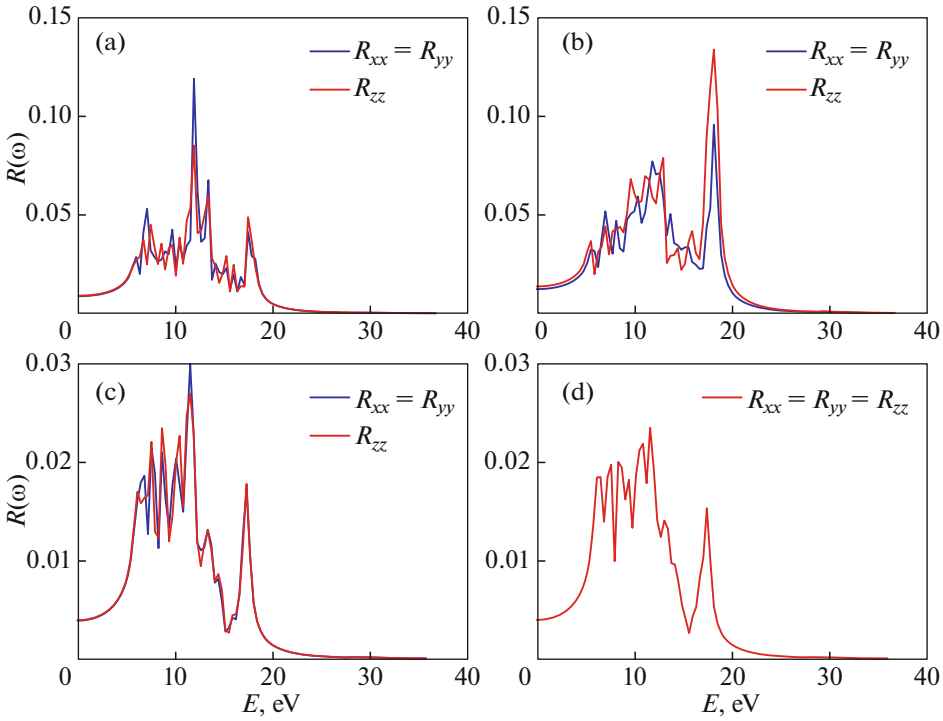

Fig. 3. Reflection functions of ices (a) I_h and (b) I_{II}, and hydrates (c) sH and (d) sI.

rial, show maxima in the energy range of 6.2–6.5 eV and minima in the ranges of 12–13 and 17–18 eV. The maximum value of dielectric function $\varepsilon'_{ik}(\omega)$ is 2.2 in the case of ices and 1.7 in the case of hydrates. In the low-energy limit, ice I_h is characterized by the $\varepsilon_1(\omega)$ value equal to 1.47; for ice I_{II}, this value is 1.61; for hydrates sI and sH, $\varepsilon_1(\omega) = 1.29$. In the high-energy limit, dielectric function $\varepsilon'_{ik}(\omega)$ tends to unity. Dielectric function $\varepsilon''_{ik}(\omega)$, which characterizes the energy loss of electromagnetic radiation in the medium, has nonzero values for ices and hydrates only in the energy range of 4–20 eV and consists of many overlapping peaks. The peaks of the $\varepsilon''_{ik}(\omega)$ function correspond to transitions between the 2*p* electrons of oxygen and the 1*s* electrons of hydrogen of water molecules in the crystal lattice [17]. The maximum intensities of the $\varepsilon''_{ik}(\omega)$ function 1.4 and 1.5 in the case of ices I_{II} and I_h, and 0.64 and 0.68 in the case of hydrates sI and sH, respectively.

5. OPTICAL FUNCTIONS

The $\varepsilon'_{ik}(\omega)$ and $\varepsilon''_{ik}(\omega)$ dielectric functions make it possible to calculate many important optical characteristics of a medium. The following frequency-dependent functions were obtained using formulas (3)–(7) [30] for ices I_h and I_{II}, and hydrates sI and sH: reflection $R(\omega)$ (see Fig. 3), absorption $a(\omega)$ (Fig. 4), real part $n(\omega)$ of the refractive index (Fig. 5), imaginary part $k(\omega)$ of the refractive index (Fig. 6), and function $L(\omega)$ of dielectric losses (see Fig. 7). The formulas are given in the system of units, in which $c = 1$

$$R(\omega) = \left|\frac{\sqrt{\varepsilon'(\omega) + i\varepsilon''(\omega)} - 1}{\sqrt{\varepsilon'(\omega) + i\varepsilon''(\omega)} + 1}\right|^2, \quad (3)$$

$$a(\omega) = \sqrt{2}\omega\left[\sqrt{\varepsilon'^2(\omega) + \varepsilon''^2(\omega)} - \varepsilon'(\omega)\right]^{1/2}, \quad (4)$$

$$n(\omega) = \frac{1}{\sqrt{2}}\left[\sqrt{\varepsilon'^2(\omega) + \varepsilon''^2(\omega)} + \varepsilon'(\omega)\right]^{1/2}, \quad (5)$$

$$k(\omega) = \frac{1}{\sqrt{2}}\left[\sqrt{\varepsilon'^2(\omega) + \varepsilon''^2(\omega)} - \varepsilon'(\omega)\right]^{1/2}, \quad (6)$$

$$L(\omega) = \varepsilon''(\omega)/\left[\varepsilon'^2(\omega) + \varepsilon''^2(\omega)\right]. \quad (7)$$

Reflection functions $R(\omega)$ in Fig. 3 demonstrate that the light reflected from ices and hydrates is predominantly distributed in the ultraviolet region (5–20 eV). Such behavior of the distribution is also valid for other optical properties. The absorption peaks of the $a(\omega)$ function at energy levels of 11.5–11.8 eV correspond to the transition of the 2*p* electrons of water.

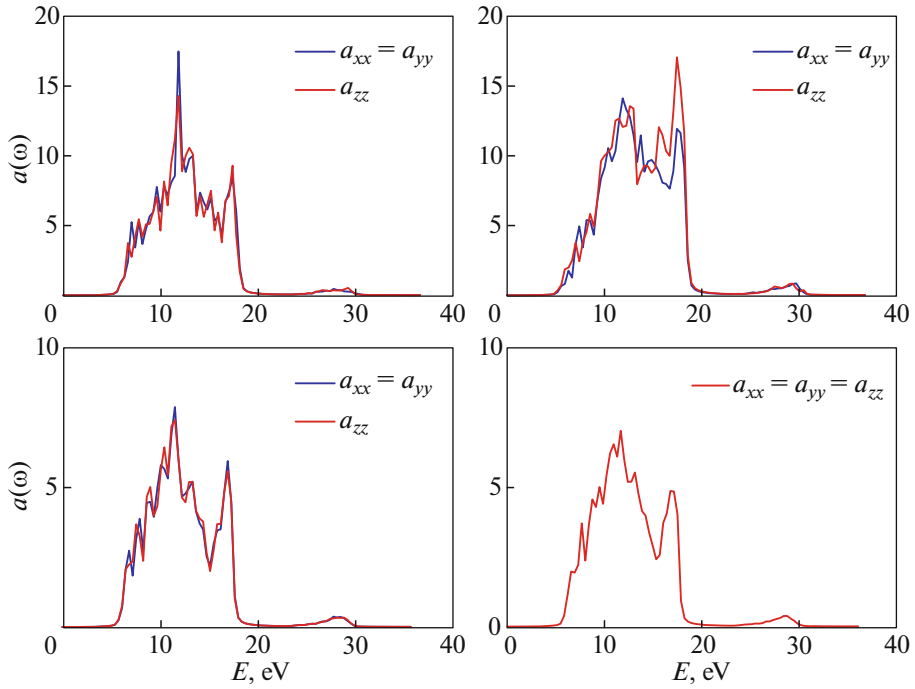

Fig. 4. Absorption functions of ices (a) I_h and (b) I_{II}, and hydrates (c) sH and (d) sI.

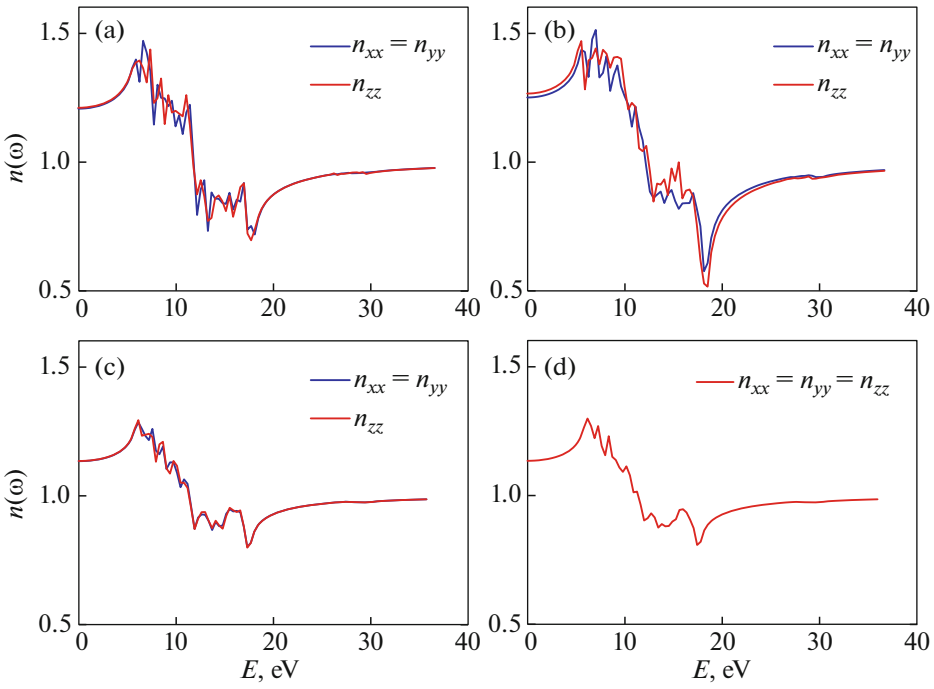

Fig. 5. Real parts of the refractive index for ices (a) I_h and (b) I_{II}, and hydrates (c) sH and (d) sI.

Refractive indices $n(\omega)$ and $k(\omega)$ replicate rather well the $\varepsilon_1(\omega)$ and $\varepsilon_2(\omega)$ spectra. The dielectric and optical functions obtained in this study for unfilled clathrate lattices sI and sH were compared with some results published in [17] (Fig. 8), in which the spectra of hydrates sI fully and partially filled with methane mol-

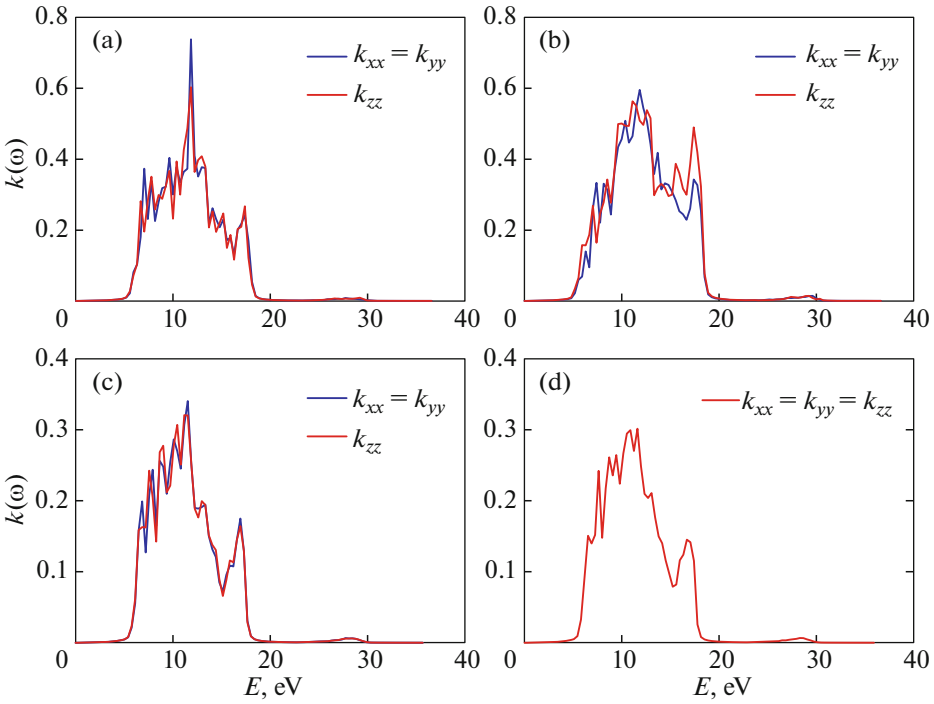

Fig. 6. Imaginary parts of the refractive index for ices (a) I_h and (b) I_{II}, and hydrates (c) sH and (d) sI.

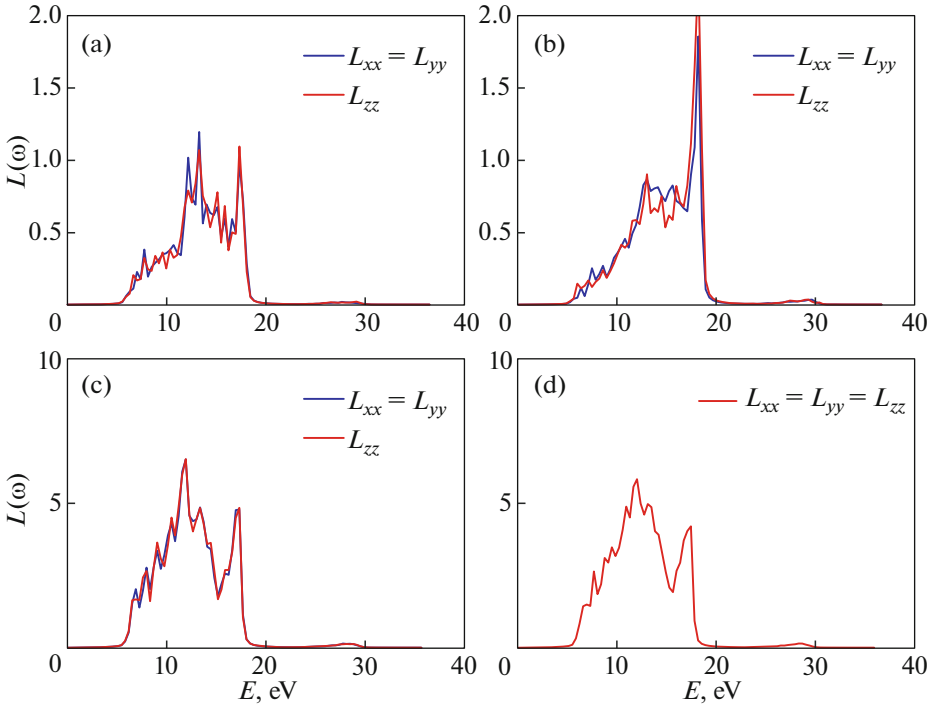

Fig. 7. Loss functions of ices (a) I_h and (b) I_{II}, and hydrates (c) sH and (d) sI.

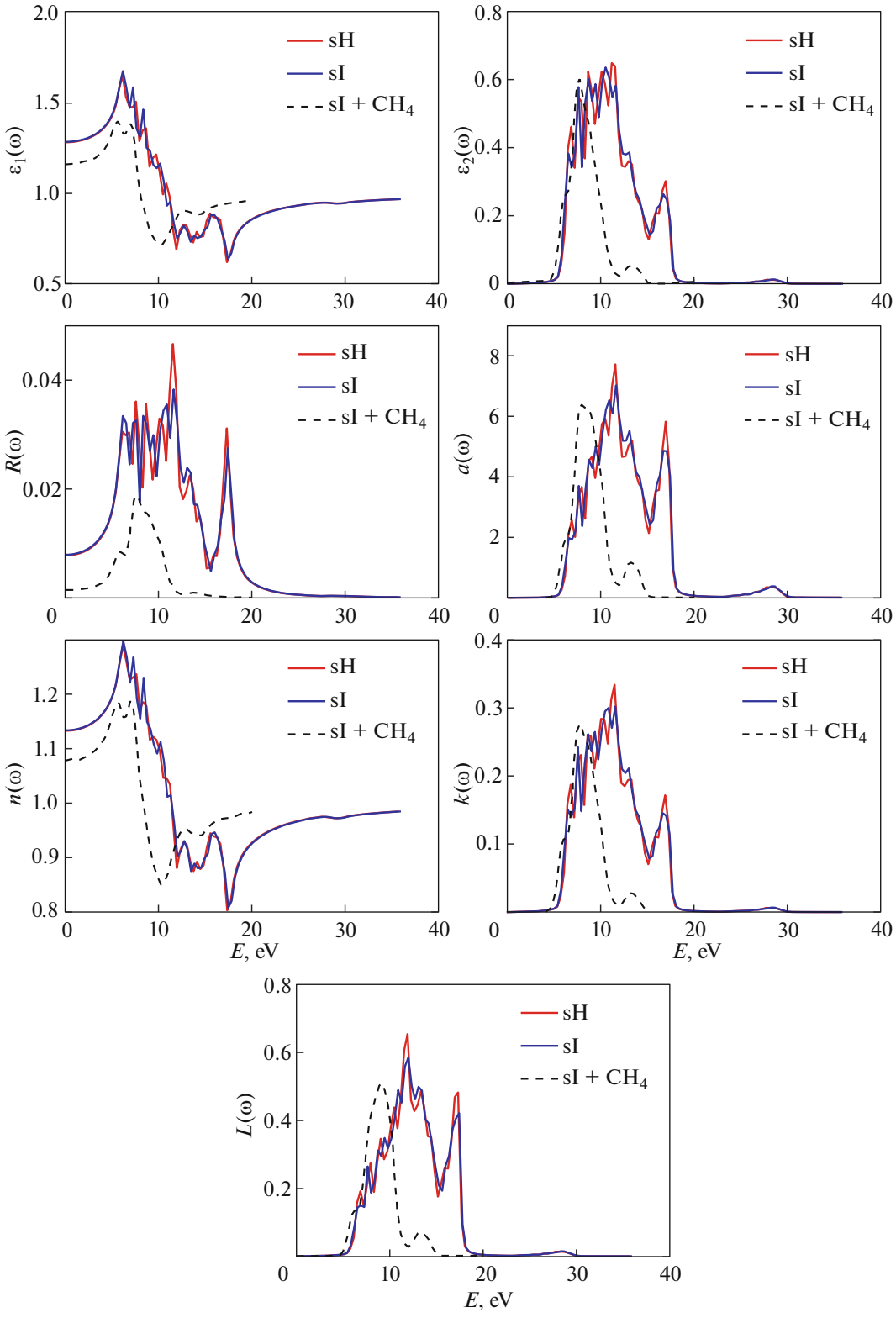

Fig. 8. Optical functions $\varepsilon_1(\omega)$, $\varepsilon_2(\omega)$, $R(\omega)$, $a(\omega)$, $n(\omega)$, $k(\omega)$, and $L(\omega)$ for unfilled hydrates sI and sH, and for gas hydrates sI with methane inclusions.

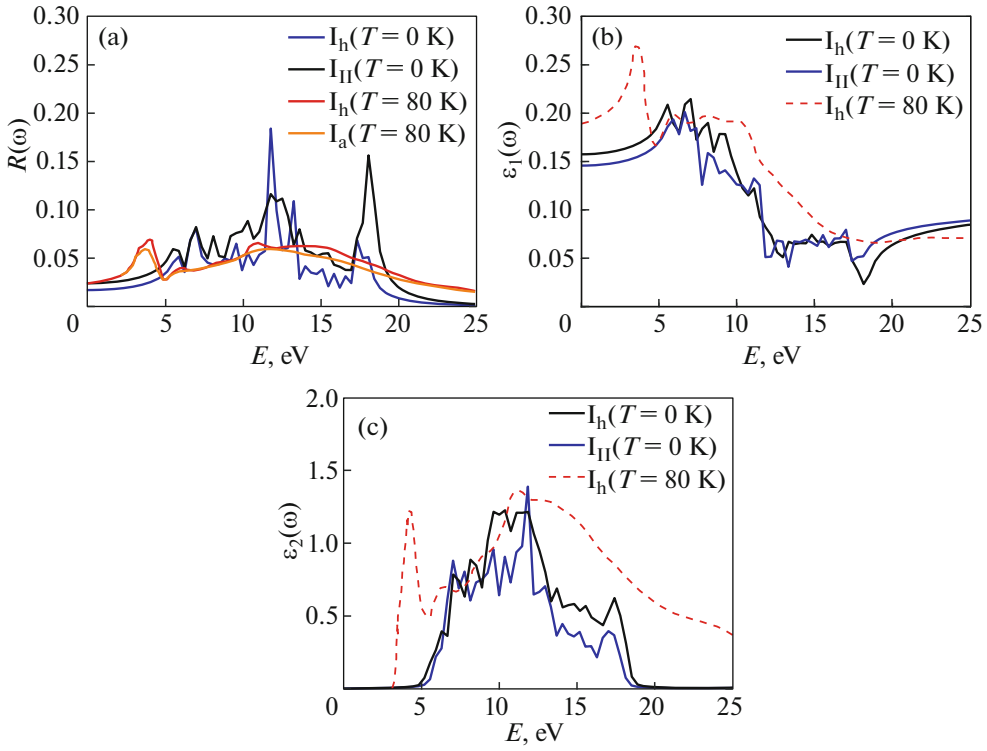

Fig. 9. Comparison of the experimental and calculated dielectric and optical spectra of ices I_h, I_{II}, and amorphous ice for (a) reflection functions $R(\omega)$, and dielectric functions (b) $\varepsilon_1(\omega)$ and (c) $\varepsilon_2(\omega)$.

ecules are calculated using the method of first-principles simulation.

As shown in Fig. 8, the spectra of unfilled sI and sH lattices have qualitative and quantitative differences from the spectra of the sI hydrate with the inclusion of methane in molecular cavities [17]. In this case, the optical functions of unfilled hydrates sI and sH are identical. For methane hydrate and unfilled hydrates, the $\varepsilon_1(\omega)$, $\varepsilon_2(\omega)$, $R(\omega)$, $a(\omega)$, $n(\omega)$, $k(\omega)$, and $L(\omega)$ spectra show the coincidence in the left boundaries of the distributions. The optical spectra of water frameworks sI and sH are more extended in the direction of high energies. The shift of the far right extrema in all spectra was about 3.5 eV. Such changes in the shape of the spectra can be associated with the structural deformations of the clathrate cavities of the hydrate with inclusion of gas molecules and with a change in the electronic structure of the hydrate crystal. It is worth paying attention to the $R(\omega)$ reflection spectra, in which the intensity of the main peak increases and an additional reflection peak appears at an energy of 17.3 eV for unfilled hydrate sI compared to methane hydrate sI. Presumably, the presence of this peak at 17.3 eV for the empty sI framework is associated with the transitions of the 2*p* electrons of water in unfilled molecular cavities. The presence of guest methane molecules has an effect on the electronic structure of the cavity [7] and prevents this transition. For the remaining $\varepsilon_1(\omega)$, $\varepsilon_2(\omega)$, $a(\omega)$, $n(\omega)$, $k(\omega)$, and $L(\omega)$ spectra, insignificant decreases in the peak intensities are observed in the presence of CH_4 molecules.

The calculated reflection spectra and dielectric functions of ices I_h and I_{II} were compared with the published data [21] (see Fig. 9). In this study, the $R(\omega)$ spectra of reflection from the surfaces of hexagonal and amorphous ice crystallized in vacuum are measured under the influence of synchrotron radiation. Next, dielectric functions $\varepsilon_1(\omega)$ and $\varepsilon_2(\omega)$ are obtained using the Kramers–Kronig relations [31]. The spectroscopy data of the system are obtained at $T = 80$ K, while quantum mechanical calculations are performed for the ground state of the system at $T = 0$ K. In addition, experimental samples may contain defects and impurities. Despite this, good qualitative and quantitative agreement is obtained between the experimental and calculated spectra, in particular, for the $\varepsilon_2(\omega)$ dielectric function. The first maxima in the $R(\omega)$ spectra of experimental samples are located at a level of 3.7 eV; in the calculated spectra, these peaks are less pronounced and are characterized by an energy of 5.6 eV. In the experimental $\varepsilon_1(\omega)$ and $\varepsilon_2(\omega)$ spectra of hexagonal ice, the first maxima are at levels of 3.7 and 4.2 eV, respectively. In addition, the experimental spectral maxima are more pronounced than those obtained in the calculated spectra, in which the corre-

sponding peaks are characterized by energies of 5.6 and 7.0 eV, respectively.

6. CONCLUSIONS

As a result of numerical quantum mechanical calculations performed for ices I_h, I_{II} and lattice frameworks of hydrates sI and sH, static dielectric tensors ε_{ik} (Table 2) in the diagonal form are obtained. It is shown that the dielectric and optical properties of I_h, I_{II}, and sH correspond to an uniaxial crystal whose main optical axis coincides with unit cell vector **c** (see Fig. 1), and the properties of ice sI correspond to a cubic isotropic crystal. The complex components of frequency-dependent dielectric function $\varepsilon_{ik}(\omega)$ are calculated in the energy range of $E \in [0; 40]$ eV (see Fig. 2), and good agreement with the published calculated data [17] is obtained. The following optical characteristics of the crystals under study are calculated based on the dielectric functions: reflection $R(\omega)$, absorption $a(\omega)$, refractive indices $n(\omega)$ and $k(\omega)$, and loss function $L(\omega)$ (see Figs. 3–7). Reflection functions $R(\omega)$ show that the light reflected from ices and hydrates is predominantly distributed in the near ultraviolet region (5–20 eV). Good agreement is found between the optical spectra of hydrate lattices sI and sH, and methane hydrate sI [17]; an additional reflection peak at an energy of 17.3 eV, which is absent in the spectrum of the methane filled hydrate, is found in the optical spectra of unfilled frameworks sI and sH (see Fig. 8). Presumably, the presence of a peak at 17.3 eV is associated with the transitions of the 2*p* electrons of water in unfilled molecular cavities. The presence of guest methane molecules has an effect on the electronic structure of the cavity and prevents this transition. Calculated reflection spectra $R(\omega)$ and functions $\varepsilon_1(\omega)$ and $\varepsilon_2(\omega)$ of ices are correlated with experimental data for hexagonal and amorphous ices (see Fig. 9). The quantum mechanical simulation results demonstrate qualitative and quantitative agreement with the published experimental spectroscopy data [21]. The optical characteristics of polymorphic phases I_h, I_{II}, sI, and sH of water, which are obtained in this study, are of fundamental and practical importance both for modern science and the energy industry. Thus, the results of this study can contribute to the development of technologies for the exploration and analysis of gas hydrate deposits.

ACKNOWLEDGMENTS

The authors are grateful to Prof. Anatolii Vasil'evich Mokshin, Dr. Sci. (Phys.–Math.), for useful discussions and valuable comments.

FUNDING

Large scale quantum mechanical calculations were performed on the computing cluster of the Kazan (Volga Region) Federal University. This work was supported by the Russian Science Foundation (project no. 22-22-00508).

CONFLICT OF INTEREST

The authors declare that they have no conflicts of interest.

REFERENCES

1. M. Cogoni, B. D'Aguanno, L. N. Kuleshova, and D. W. M. Hofmann, J. Chem. Phys. **134**, 204506 (2011).
2. E. D. Sloan and C. A. Koh, *Clathrate Hydrates of Natural Gases* (CRC, Boca Raton, FL, 2007).
3. J. D. Bernal and R. H. Fowler, J. Chem. Phys. **1**, 420 (1933).
4. A. D. Fortes, I. G. Wood, J. P. Brodholt, and L. Vocadlo, J. Chem. Phys. **119**, 4567 (2003).
5. R. K. Zhdanov, V. R. Belosludov, Yu. Yu. Bozhko, O. S. Subbotin, and K. V. Gets, JETP Lett. **108**, 806 (2018).
6. R. M. Khusnutdinoff, Colloid J. **75**, 726 (2013).
7. M. B. Yunusov and R. M. Khusnutdinov, Uch. Zap. Fiz. Fak. Mosk. Univ., No. 4, 2240702 (2022).
8. J. H. van der Waals, Trans. Faraday Soc. **52**, 184 (1956).
9. F. A. Kuznetsov, V. A. Istomin, and T. V. Rodionova, Ros. Khim. Zh. **47**, 5 (2003).
10. F. Su, C. L. Bray, B. O. Carter, G. Overend, C. Cropper, J. A. Iggo, and A. I. Cooper, Adv. Mater. **21**, 2382 (2009).
11. F. Takeuchi, M. Hiratsuka, R. Ohmura, S. Alavi, A. K. Sum, and K. Yasuoka, J. Chem. Phys. **138**, 124504 (2013).
12. A. Yu. Monakov and Yu. A. Dyadin, Ros. Khim. Zh. **47** (3), 28 (2003).
13. M. B. Yunusov, R. M. Khusnutdinoff, and A. V. Mokshin, Phys. Solid State **63**, 372 (2021).
14. M. B. Yunusov and R. M. Khusnutdinoff, J. Phys.: Conf. Ser. **2270**, 012052 (2022).
15. J. E. Jing, K. Chen, M. Deng, Q. X. Zhao, X. H. Luo, G. H. Tu, and M. Wang, J. Asian Earth Sci. **171**, 201 (2019).
16. J. F. Wright, F. M. Nixon, and S. R. Dallimore, in *Proceedings of the 4th International Conference on Gas Hydrates* (2002).
17. Z. Wang, L. Yang, R. Deng, and Z. Yang, arXiv: 1902.10914 (2019).
18. K. Takeya, M. Tonouchi, and K. Ohgaki, in *Proceedings of the 6th International Conference on Hydrates* (2008).
19. K. Takeya, C. Zhang, I. Kawayama, H. Murakami, P. U. Jepsen, J. Chen, and M. Tonouchi, Appl. Phys. Express **2**, 122303 (2009).
20. S. Takeya and J. A. Ripmeester, in *Proceedings of the 7th International Conference on Gas Hydrates* (2011).

21. K. Kobayashi, J. Phys. Chem. **87**, 4317 (1983).
22. P. Hohenberg and W. Kohn, Phys. Rev. **136**, 864 (1964).
23. W. Kohn and L. J. Sham, Phys. Rev. A **140**, 1133 (1965).
24. G. Kresse and J. Furthmuller, Phys. Rev. **54**, 11169 (1996).
25. G. Kresse and D. Joubert, Phys. Rev. **59**, 1758 (1999).
26. J. P. Perdew, *Electronic Structures of Solids'91* (Akademie Verlag, 1991).
27. J. P. Perdew, K. Burke, and M. Ernzerhof, Phys. Rev. Lett. **77**, 3865 (1996).
28. P. Pulay, Chem. Phys. Lett. **73**, 393 (1980).
29. L. D. Landau and E. M. Lifshitz, *Course of Theoretical Physics,* Vol. 8: *Electrodynamics of Continuous Media* (Fizmatlit, Moscow, 2005; Pergamon, New York, 1984).
30. L. Sun, X. Zhao, Y. Li, P. Li, H. Sun, X. Cheng, and W. Fan, J. Appl. Phys. **108**, 093519 (2010).
31. P. Y. Yu and M. Cardona, *Fundamentals of Semiconductors* (Springer, Berlin, 1996).

Translated by O. Kadkin